

NMR investigations of quantum battery using star-topology spin systems

Jitendra Joshi* and T S Mahesh†

Department of Physics and NMR Research Center,
Indian Institute of Science Education and Research, Pune 411008, India

Theoretical explorations have revealed that quantum batteries can exploit quantum correlation to achieve faster charging, thus promising exciting applications in future technologies. Using NMR architecture, here we experimentally investigate various aspects of quantum battery with the help of nuclear spin systems in star-topology configuration. We first carry out numerical analysis to study how charging a quantum battery depends on the relative purity factors of charger and battery spins. By experimentally measuring the polarization of the battery spin undergoing charging, we estimate the battery energy and establish the theoretically predicted quantum advantage. We propose using the quantum advantage, which depends on the entanglement among chargers and battery, as a measure for estimating the size of the entangled cluster. We develop a simple iterative method to realize asymptotic charging avoiding oscillatory behaviour of charging and discharging. Finally, we introduce a load spin and realize a charger-battery-load circuit and experimentally demonstrate battery energy consumption after varying durations of battery storage, for up to two minutes.

I. INTRODUCTION

Recent advances in quantum technologies are revolutionizing world with novel devices such as quantum computers, quantum communication, quantum sensors, and a host of other quantum-enhanced applications [1, 2]. The latest additions include quantum engines [3–5], quantum diode [6, 7], quantum transistor [8], as well as quantum battery, an energy-storing device [9–16] that is capable of exploiting quantum superpositions [17–22]. While quantum batteries open up novel applications, they are also exciting from the point of view of quantum thermodynamics [23–25], a rapidly emerging field that extends thermodynamical concepts to the quantum regime. It has been theoretically established that quantum batteries can exhibit faster charging in a collective charging scheme that exploits entanglement [18, 19]. Recently quantum batteries with various models showing quantum advantages have been introduced [26, 27]. They include quantum cavity [10, 20, 28–34], spin chain [35–41], Sachdev-Ye-Kitaev model [42, 43], and quantum oscillators [9, 21, 44, 45]. There also have been a few experimental investigations of quantum battery, such as the cavity assisted charging of an organic quantum battery [46].

Here we describe an experimental exploration of quantum batteries formed by nuclear spins systems of various sizes in star-topology configuration. Using NMR methods, we study various aspects of quantum battery. First we experimentally measure build up of battery energy during collective charging and establish the quantum speedup. By quantifying entanglement in terms of entanglement entropy as well as discord, we reconfirm the involvement of entanglement in yielding the quantum speedup. We therefore proposed using the quan-

tum speed up as a measure of size of the entangled cluster. We find this method to be much simpler compared to spatial phase-encoding method [47] or the temporal phase-encoding method (eg. [48]). Unlike classical batteries, charging of a quantum battery is oscillatory, i.e., the quantum battery starts discharging after reaching the maximum charge. Recent theoretical proposals to realize a stable non-oscillatory charging were based on either adiabatic protocol [49] or shortcut to adiabaticity [50]. Here we propose and demonstrate a simple iterative procedure to realize asymptotic charging based on the differential storage times of the charger and battery spins. Finally, we describe implementing the Quantum Charger-Battery-Load (QCBL) circuit. A similar circuit has recently been theoretically discussed in Ref. [51]. Using a 38-spin star-system we experimentally demonstrate QCBL circuit with battery storage up to two minutes before discharging energy on to the load spin.

The article is organised as follows. In Sec. II, we describe the theoretical modeling of quantum battery and describe the numerical analysis of battery performance in terms of relative purity factors of charger and battery spins. In Sec. III, we describe the following experimental studies on quantum battery. The study of quantum advantage is reported in Sec. IIIA. The proposal to use quantum advantage as a measure of cluster size is discussed in Sec. IIIB. The scheme to avoid oscillatory charging is described in Sec. IIIC. Finally, we describe implementation of the QCBL circuit in Sec. IIID before summarizing in Sec. IV.

II. THEORY

A. A nuclear spin-battery

The simplest quantum battery (B) consists of a two-level quantum system, like a spin-1/2 particle placed in a magnetic field (Fig. 1). Here, the ground state $|0\rangle$ is modeled as a discharged or empty battery, while the

* jitendra.joshi@students.iiserpune.ac.in

† mahesh.ts@iiserpune.ac.in

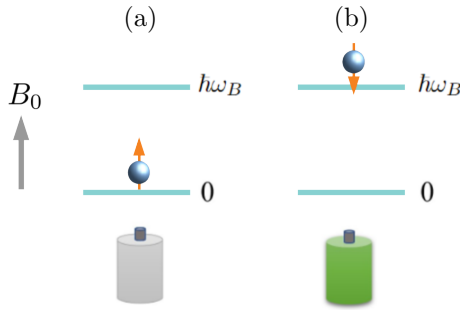


FIG. 1. A single spin-1/2 particle in an external magnetic field B_0 as a quantum battery. The ground state (a) and excited state (b) correspond respectively to uncharged and charged states of the battery.

excited state $|1\rangle$ is modeled as the fully charged battery. The spin battery can be charged either directly using an external drive [18, 20] or indirectly via an ancillary spin, called charger spin (C) [35, 51]. Let us now consider the B-C spin system. Each of the two spins are governed by their local Hamiltonians H_B and H_C , respectively, which for the sake of simplicity, are chosen to have zero ground-state energy. Moreover, we assume that the quantum system at an initial time $t = 0$ is in a factorized state

$$\rho_{BC}(0) = |0\rangle\langle 0|_B \otimes |1\rangle\langle 1|_C, \quad (1)$$

with $|1\rangle\langle 1|_C$ being the excited state of the charger.

We now introduce a coupling Hamiltonian $H_{BC}(t)$ between B and C, in order to transfer as much energy as possible from the charger to the battery over a finite charging duration τ . Under the global Hamiltonian of the system BC

$$H(t) = H_B + H_C + H_{BC}(t), \quad (2)$$

the joint system evolves as

$$\rho_{BC}(\tau) = U(\tau)\rho_{BC}(0)U^\dagger(\tau) \text{ with } U(\tau) = Te^{-i\int_0^\tau dt H(t)}, \quad (3)$$

where T is the time-ordering operator. The instantaneous state of battery $\rho_B(\tau) = \text{Tr}_C(\rho_{BC}(\tau))$ is obtained by tracing out the charger. The goal is to maximize the local energy of the battery

$$E_B^{\max} = E_B(\bar{\tau}) = \text{Tr}(\rho_B(\bar{\tau})H_B), \quad (4)$$

with the shortest possible charging time $\bar{\tau}$. For a given maximum energy charged E_B^{\max} , the charging power is defined as $P = E_B^{\max}/\bar{\tau}$.

We now discuss two charging schemes, parallel and collective [18, 20, 35] as illustrated in Fig. 2. In parallel charging scheme, each of the N batteries is independently charged to a maximum energy E_B^{\max}/N by one of the N chargers over a duration $\bar{\tau}_1$. Conversely, in the collective charging scheme, all the batteries together form a battery-pack that is charged to a maximum energy E_B^{\max}

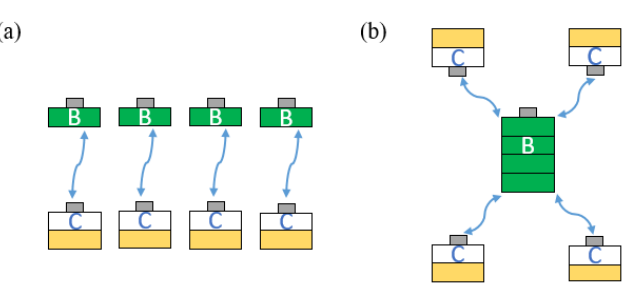


FIG. 2. Two charging schemes: (a) parallel charging scheme where a single battery is charged by an individual charger and (b) the collective charging scheme where a single battery is charged by multiple chargers.

simultaneously by N chargers over a duration $\bar{\tau}_N$. The latter scheme exploits quantum entanglement and hence is more efficient [18, 20]. Let P_1 and P_N be the the charging powers of the parallel and collective charging schemes respectively. The quantum advantage of collective charging is defined as [19]

$$\Gamma \equiv \frac{P_N}{P_1} = \frac{E_B^{\max}/\bar{\tau}_N}{N(E_B^{\max}/N)/\bar{\tau}_1} = \frac{\bar{\tau}_1}{\bar{\tau}_N}. \quad (5)$$

B. Star-topology network

We now consider the star-topology network in which a single central battery-spin uniformly interacts with a set of N indistinguishable charger spins [52] as illustrated in Fig. 3 (a). Quantum battery in this configuration has been studied theoretically very recently [53]. The spin-systems with $N = 3, 9, 12, 18, \& 36$ studied in this work are shown in Fig. 3 (b-f).

We consider the local Hamiltonians for the battery and charger to be

$$H_B = \hbar\omega_B(1/2 - S_z) \text{ and } H_C = \hbar\omega_C I_z. \quad (6)$$

Here $S_{x,y,z}$ represent the x, y, z -spin operators for the battery spin with Larmor frequency ω_B , $I_{x,y,z} = \sum_{i=1}^N I_{x,y,z}^i$ represent the collective x, y, z -spin operators for the chargers with Larmor frequency $\omega_C = \gamma\omega_B$, where γ is the relative gyromagnetic ratio. Following Ref. [21], we choose the interaction Hamiltonian,

$$H_{BC}(t) = \hbar 2\pi J (S_x I_x + S_y I_y), \quad (7)$$

where $J \ll |\omega_{C(B)}|$ is the coupling constant between the battery and the charger spins.

The spin-system is prepared in the thermal equilibrium

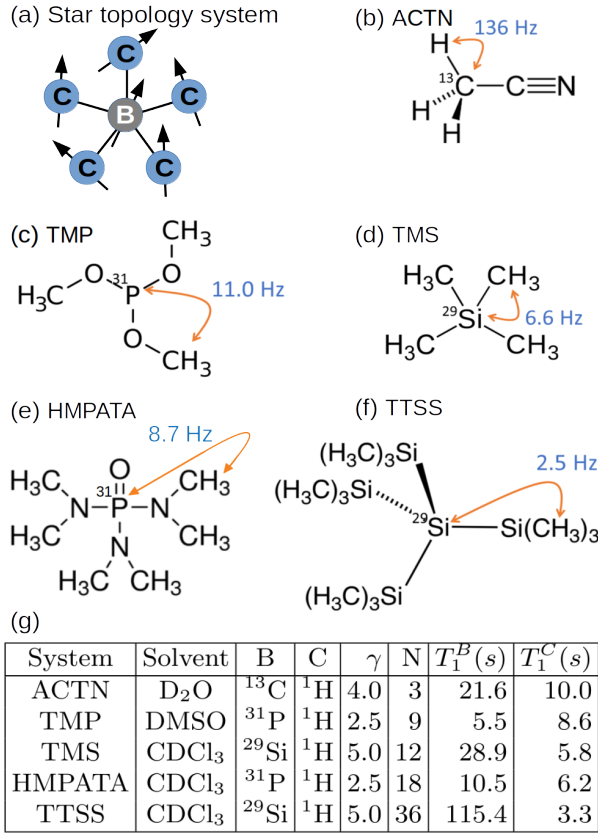


FIG. 3. (a) Star-topology configuration showing the central battery spin symmetrically surrounded by charger spins. (b-f) The star-topology nuclear spin-systems studied in this work. The strength J of battery-charger interaction for each system is shown with the molecular structure, while other details are tabulated in (g).

state, which is in a generalized form of Eq. 1, i.e.,

$$\rho_{BC}(0) = \rho_B(0) \otimes \rho_C(0), \text{ with}$$

$$\rho_B(0) = \frac{1+\epsilon}{2} |0\rangle\langle 0| + \frac{1-\epsilon}{2} |1\rangle\langle 1| \text{ and}$$

$$\rho_C(0) = \left(\frac{1-\gamma\epsilon}{2} |0\rangle\langle 0| + \frac{1+\gamma\epsilon}{2} |1\rangle\langle 1| \right)^{\otimes N}, \quad (8)$$

where ϵ and $\gamma\epsilon$ are the purity factors of the battery and charger spins respectively.

We evolve the whole system for a duration τ under the total Hamiltonian in the interaction frame defined by $U_{\text{IF}}(t) = e^{-i(H_B+H_C)t/\hbar}$. The dimensionless energy of the battery

$$e_B(\tau) = E_B(\tau)/\hbar\omega_B = \langle 1 | \rho_B(\tau) | 1 \rangle \quad (9)$$

is related to the normalized polarization of the battery

$$m_B(\tau) = \langle \sigma_z \rangle_{\rho_B(\tau)} / \epsilon \quad \text{via} \quad e_B(\tau) = \frac{1 - m_B(\tau)}{2}. \quad (10)$$

For the special case of pure state, i.e., $\epsilon = 1$ and also

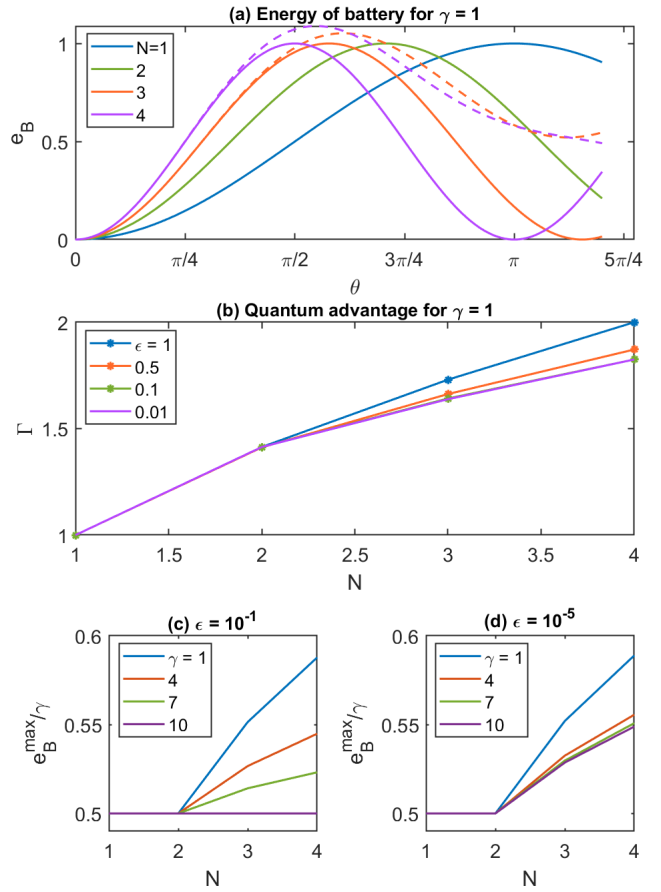


FIG. 4. (a) Battery energy e_B versus charging phase $2\pi J\tau$ for different number N of chargers in pure (solid lines) as well as mixed (dashed lines; $\epsilon = 10^{-5}$) state cases. (b) Quantum advantage Γ versus N for different purity values ϵ . (c-d) e_B^{\max}/γ versus N for different γ values at $\epsilon = 10^{-1}$ (c) and $\epsilon = 10^{-5}$ (d).

setting $\gamma = 1$, we obtain the dimensionless energy

$$e_B(\tau) = \sin^2(\sqrt{N}\theta/2) \text{ in terms of } \theta = 2\pi J\tau. \quad (11)$$

The energy is maximized for $\bar{\theta} = \pi/\sqrt{N}$ at optimal time

$$\bar{\tau}_N = \frac{\bar{\theta}}{2\pi J} = \frac{1}{2J\sqrt{N}} \quad \& \text{ therefore } \quad \Gamma = \frac{\bar{\tau}_1}{\bar{\tau}_N} = \sqrt{N}, \quad (12)$$

clearly predicting the quantum speed-up. The battery energy evolution for various numbers of charger spins are shown in Fig. 4 (a). Note that mixed state curves deviate from the pure state curves for $N \geq 3$. Here, while e_B exceeds the pure state value of unity, the maximum charging takes longer duration. The quantum advantage Γ versus number of charger spins for $\gamma = 1$ and various values of ϵ are shown in Fig. 4 (b). Note that for mixed state cases $\Gamma < \sqrt{N}$. One may naively imagine that the maximum battery energy e_B^{\max} scales linearly with γ .

However, the plots of e_B^{\max}/γ plotted versus γ in Fig. 4 (c) and (d) show the nonlinear dependence, especially for $N \geq 3$ and for smaller values of γ .

III. EXPERIMENTS

A. Establishing quantum advantage

Our first aim is to establish the quantum advantage described in section II B using various systems shown in Fig. 3. The table containing information about the solvent, the relative gyromagnetic ratio (γ), and the T_1 relaxation time constant for each of the spin systems is shown in Fig. 3 (g). All the experiments were carried out in a 500 MHz Bruker NMR spectrometer at an ambient temperature of 298 K. The NMR pulse-sequence for the experiments is shown in Fig. 5 (a). Starting from thermal equilibrium state, we energize the charger spin by inverting its population with the help of a π pulse. This is followed by the charging propagator

$$U_{XY}(\tau/n_0) = e^{-iH_{BC}\tau/n_0} \approx Y \cdot ZZ \cdot Y^\dagger \cdot X \cdot ZZ \cdot X^\dagger. \quad (13)$$

Here, $X(Y) = e^{-i(S_{x(y)} + I_{x(y)})\pi/2}$ and $ZZ = e^{-iS_z I_z \theta/m}$. Note that for $N \geq 2$, $[S_x I_x, S_y I_y] \neq 0$, and therefore we implement the interaction propagator via integral iterations $n \in [0, n_0]$ of $U_{XY}(\tau/n_0)$ with sufficiently large n_0 such that $\tau/n_0 \ll 1/(2J)$. Finally, after dephasing spurious coherences with the help of a pulsed-field-gradient (PFG), we apply a $\pi/2$ detection pulse and measure the battery polarization $m_B(\tau)$. During the detection period, we decouple charger spins using WALTZ-16 composite pulse sequence [54].

The experimentally measured battery energy e_B (estimated from m_B using Eq. 10 for all five spin-systems shown in Fig. 3) are plotted versus normalized charging duration $\tau/\bar{\tau}_N$ in Fig. 5 (b). For an ideal pure-state system, we expect the maximum energy storage at $\tau/\bar{\tau}_N = 1$. On the other hand, for mixed state systems with $N \geq 3$, $\tau/\bar{\tau}_N$ slightly overshoots the unit value. However, in practical systems, the charging dynamics is affected by the experimental imperfections such as field inhomogeneity, off-set and calibration errors, etc. In spite of these issues, the results shown in Fig. 5 (b) for all the systems show a remarkable agreement with the expected maximum charging duration at $\bar{\tau}_N$. The corresponding quantum advantage Γ for all the systems are plotted versus the number N of charger spins in Fig. 5 (c), where the solid line corresponds to the theoretically expected \sqrt{N} function. Clearly, we observe a significant quantum advantage ranging from about 1.5 to over 6.

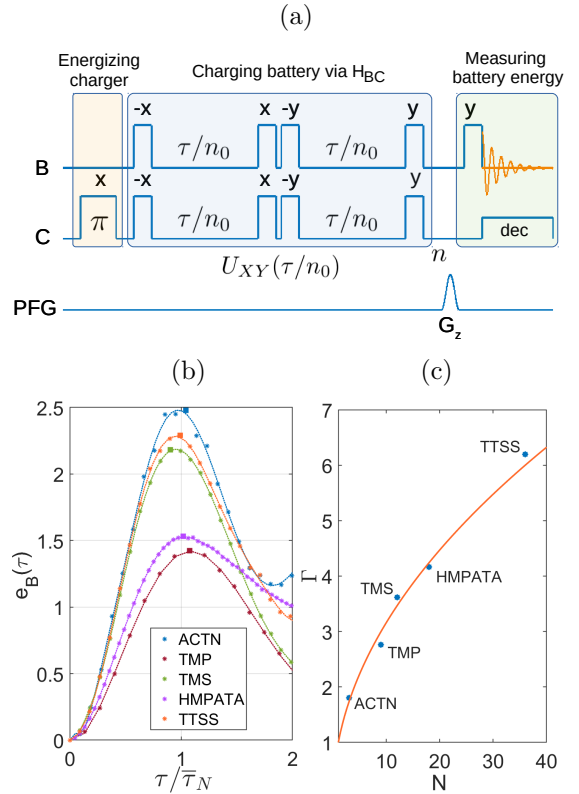


FIG. 5. (a) The NMR pulse sequence for charging quantum battery and measuring its energy. The wide and narrow rectangular pulses correspond to π and $\pi/2$ pulses respectively. The shaped pulse in the lowest row corresponds to the pulsed-field-gradient (PFG) which destroys the coherences and retains populations. (b) The battery energy e_B versus normalized charging duration $\tau/\bar{\tau}_N$ for the five spin systems shown in Fig. 3. (c) Quantum advantage Γ versus the number N of charger spins showing \sqrt{N} dependence.

B. Determining size of the entangled cluster

It has been shown that charging quantum battery via collective mode generates entanglement [18]. The same holds true for charging in the star-topology system. In Fig. 6, we plot entanglement entropy as well as quantum discord against the normalized charging time $\tau/\bar{\tau}_9$ for a star-system with $N = 9$ charger spins. For reference we also show the charging energy e_B for both pure (with $\epsilon = 1$, $\gamma = 1$) and mixed state (with $\epsilon = 10^{-5}$, $\gamma = 1$). To evaluate entanglement entropy we traced out charger spins, and evaluated the von Neumann entropy of the battery state. For evaluating quantum discord, we used the two-spin reduced state obtained by tracing out all spins except the battery spin and one of charger spins. We find that the maximum correlation is reached at $\tau/\bar{\tau}_9 = 0.5$, i.e., at half the maximum charging period. Both entanglement entropy and discord vanish at maximum charging period, i.e., $\tau/\bar{\tau}_9 = 1$, and the spins get uncorrelated [17, 18]. Since (i) the quantum advantage is linked to the generation of entangled state [18] and

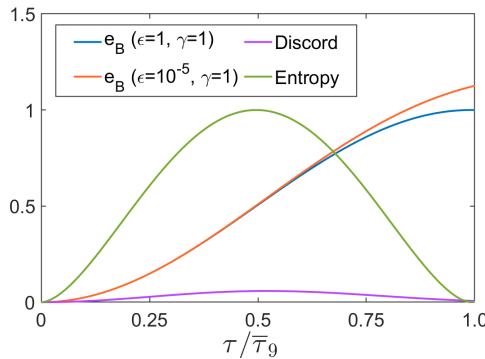


FIG. 6. Numerically calculated battery energy (with pure and mixed states), entanglement entropy (for pure state; $\epsilon = 1$, $\gamma = 1$), and quantum discord (for mixed state; $\epsilon = 10^{-5}$, $\gamma = 1$) versus the normalized charging duration $\tau/\bar{\tau}_9$ for $N = 9$ star-system involving a single battery spin and nine charger spins.

(ii) the maximum charging period depends on the size of the entangled cluster, here we propose to use $\Gamma^2 + 1$ as the lower bound for size of the entangled cluster. This measure is justified by the excellent agreement between the theory and experiment for all the five systems investigated in Fig. 5 (b) and (c). For example, the experimentally obtained value $\Gamma \approx 6$ for TTSS confirms an entangled cluster of 37 spins.

C. Asymptotic charging

We now propose a simple method to avoid oscillatory charging and realize an asymptotic charging that keeps the quantum battery from discharging. The method relies on the differential storage times of the charger and the battery spins, i.e., $T_1^B \gg T_1^C$. It involves iteratively re-energizing the chargers followed by transferring the charge to the quantum battery after a carefully chosen delay. The scheme for the asymptotic charging is described by the pulse-sequence shown in Fig. 7 (a). It involves a delay Δ before energizing the charger followed by charging the battery. However, unlike the unitary scheme described in section III A, here the entire process including waiting time, re-energizing of the battery, and charging is iterated. The experimentally measured battery energy e_B of the asymptotic charging with TTSS system are shown by dots in Fig. 7 (b), wherein the dashed lines represent the fits to asymptotic charging functions $e_B(n\Delta) = e_B^\Delta(1 - e^{-n\Delta/T_\Delta})$. Note that for TTSS, $T_1^B = 115.4$ s which is much longer than $T_1^C = 3.3$ s (see Fig. 3 (g)). The estimated values of the charging time-constants T_Δ is plotted versus Δ in the inset of Fig. 7 (b). It is clear that there is an optimal delay time Δ for which we observe maximum charging. Therefore, we monitored the saturation charging, i.e., $e_B(20\Delta)$ versus the delay time Δ as shown in Fig. 7 (c). For TTSS, we find the optimal delay ranges from 7.5 s to 10 s, to

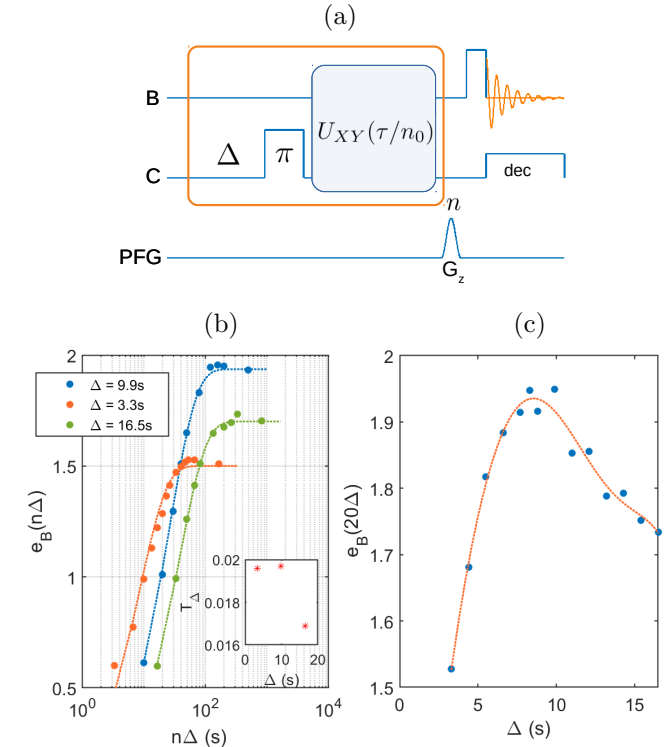


FIG. 7. (a) The NMR pulse sequence for asymptotic charging of a quantum battery. (b) Battery energy e_B versus charging duration $n\Delta$ for three values of delay Δ . The charging time-constants for these three cases are plotted in the inset. (c) Battery energy at saturation $e_B(20\Delta)$ (after $n = 20$ iterations) versus the delay Δ showing the optimal delay range from 7.5 s to 10 s.

asymptotically achieve over 85 % charging compared to the simple unitary method described in section III A.

D. Quantum Charger-Battery-Load (QCBL) Circuit

Now we describe the QCBL circuit consisting of charger (C), battery (B), as well as a load (L). Here we again use TTSS system, and consider all the proton spins together as charger, the central ^{29}Si spin as the battery, and the peripheral ^{29}Si spin as the load. Given the 5% natural abundance of ^{29}Si , the probability of both central and one of the four peripheral silicon nuclei to be ^{29}Si isotope is 0.2%. In this system, the strength of the ^{29}Si - ^{29}Si interaction, i.e., $J_{BL} = 52.4$ Hz. The QCBL circuit and the corresponding spin labeling are illustrated on the left of Fig. 8 (a). The NMR pulse-sequence for QCBL is shown on the right side of Fig. 8 (a). We first charge the battery (B) as described in Sec. III A and switch-off the C-B interactions by decoupling the charger spins throughout. Subsequently, we can introduce a battery storage duration τ_s , after which we apply a Gaussian spin-selective $\pi/2$ pulse on L followed by a PFG (G_{1z}). This ensures that there is no residual polarization of the

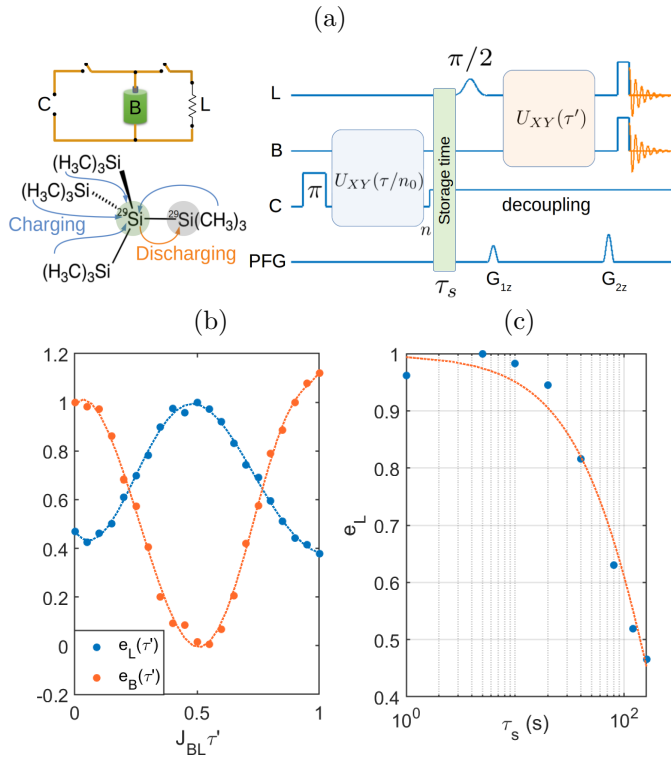


FIG. 8. (a) The QCBL circuit and its implementation in the 38-spin star-topology system (left) and the NMR pulse sequence for the QCBL circuit (right). (b) The energy of battery (e_B) and load (e_L) versus discharging parameter $J_{BL}\tau'$. (c) The energy of the load (e_L) extracted from the battery after a storage time τ_s .

load (L) spin. We now introduce the discharging scheme $U_{XY}(\tau')$ between B and L. Note that, the U_{XY} propagator can be exactly implemented in the case of two-spin interaction. Finally, we measure the polarizations of both B and L spins after destroying the spurious coherences using a second PFG G_{z2} , and thereby estimate their energies e_B and e_L respectively. The experimental results of e_B and e_L are plotted versus $J_{BL}\tau'$ in Fig. 8 (b). In our experiment, the load spin is beginning from a maximally mixed state instead of the ground state. Therefore, e_L starts with a value around 0.5 before raising towards the maximum value of 1.0 for $J_{BL}\tau' = 0.5$. At this value of $J_{BL}\tau'$, we vary the battery storage time τ_s and monitor the load energy e_L . The results are shown in Fig. 8 (c). As expected, the data fits to an exponential decay function $e^{-\tau_s/T_s}$ (dashed line in Fig. 8 (c)) with an estimated battery storage time-constant $T_s \approx 200$ s. This completes the demonstration of QCBL circuit.

IV. SUMMARY AND OUTLOOK

Considering the potential applications of quantum technologies, it is of great interest to study energy storage and usage at the quantum level. In this context, there is a significant contemporary interest in studying quantum battery. We investigated various aspects of quantum battery using nuclear spin systems in star-topology molecules in the context of NMR architecture. We first theoretically compared the efficiency of collective charging scheme (involving entanglement) with parallel (classical) scheme. Our numerical results with star-topology spin systems revealed the dependence of charging speedup as well as the maximum battery energy on relative purity factors.

Using NMR methods, we experimentally studied collective charging scheme in a variety of spin-systems, each having a single battery spin and a set of charger spins whose number N ranged between 3 and 36. By measuring the polarization of the battery spin, we estimated the battery energy and thereby established the quantum advantage $\Gamma = \sqrt{N}$ of the collective charging scheme. By numerically evaluating entanglement entropy and quantum discord for star-systems, we reconfirmed the established fact that the quantum advantage is realized via entanglement. Therefore, we proposed using $\Gamma^2 + 1$ as a lower bound for estimating the size of an entangled cluster. In particular, for a 37 spin-system, we obtained an experimental value of $\Gamma \approx 6$, which in this case matched well with the expected number.

We then addressed the issue of oscillatory charging wherein the battery starts discharging after overshooting the optimal charging duration. To this end, we proposed a simple asymptotic charging method that involves iteratively re-energizing the charger with a suitable delay. We experimentally demonstrated asymptotic charging and determined the optimal delay range.

Finally, we introduce a load spin to which the battery can deposit its energy after a suitable storage time, thus completing the complete charger-battery-load circuit. Using a 38-spin system, we show that the battery spin can store energy for up to two minutes and yet is able to transfer the stored energy to the load spin.

We believe this work paves the way for further methodology developments towards the practical aspects of quantum batteries. Such developments may also contribute towards better understanding of quantum thermodynamics and its applications. One may also envisage an advanced circuit involving multiple elements such as quantum diodes, quantum transistors, and quantum heat engines, in addition to quantum batteries.

ACKNOWLEDGEMENTS

Authors acknowledges valuable discussions with Soham, Rupak, Krithika, Priya, Arijit, and Conan. TSM acknowledges funding from DST/ICPS/QuST/2019/Q67.

[1] M. A. Nielsen and I. Chuang, “Quantum computation and quantum information,” (2002).

[2] H.-K. Lo, T. Spiller, and S. Popescu, *Introduction to quantum computation and information* (World Scientific, 1998).

[3] H.-T. Quan, Y.-x. Liu, C.-P. Sun, and F. Nori, Physical Review E **76**, 031105 (2007).

[4] R. Kosloff and A. Levy, Annual Review of Physical Chemistry **65**, 365 (2014).

[5] H. P. Goswami and U. Harbola, Physical Review A **88**, 013842 (2013).

[6] C. Palacios-Berraquero, in *Quantum Confined Excitons in 2-Dimensional Materials* (Springer, 2018) pp. 71–89.

[7] S. Nakamura, M. Senoh, S.-i. Nagahama, N. Iwasa, T. Yamada, T. Matsushita, H. Kiyoku, and Y. Sugimoto, Japanese Journal of Applied Physics **35**, L74 (1996).

[8] L. Geppert, IEEE Spectrum **37**, 46 (2000).

[9] G. M. Andolina, D. Farina, A. Mari, V. Pellegrini, V. Giovannetti, and M. Polini, Physical Review B **98**, 205423 (2018).

[10] G. M. Andolina, M. Keck, A. Mari, M. Campisi, V. Giovannetti, and M. Polini, Physical review letters **122**, 047702 (2019).

[11] J. Åberg, Nature communications **4**, 1 (2013).

[12] R. Alicki and D. Gelbwaser-Klimovsky, New Journal of Physics **17**, 115012 (2015).

[13] M. F. Frenzel, D. Jennings, and T. Rudolph, Physical review E **90**, 052136 (2014).

[14] N. Friis and M. Huber, Quantum **2**, 61 (2018).

[15] G. Francica, F. C. Binder, G. Guarneri, M. T. Mitchison, J. Goold, and F. Plastina, Physical Review Letters **125**, 180603 (2020).

[16] G. Francica, J. Goold, F. Plastina, and M. Paternostro, npj Quantum Information **3**, 1 (2017).

[17] R. Alicki and M. Fannes, Physical Review E **87**, 042123 (2013).

[18] F. C. Binder, S. Vinjanampathy, K. Modi, and J. Goold, New Journal of Physics **17**, 075015 (2015).

[19] F. Campaioli, F. A. Pollock, F. C. Binder, L. Céleri, J. Goold, S. Vinjanampathy, and K. Modi, Physical review letters **118**, 150601 (2017).

[20] D. Ferraro, M. Campisi, G. M. Andolina, V. Pellegrini, and M. Polini, Physical review letters **120**, 117702 (2018).

[21] G. M. Andolina, M. Keck, A. Mari, V. Giovannetti, and M. Polini, Physical Review B **99**, 205437 (2019).

[22] F. Campaioli, F. A. Pollock, and S. Vinjanampathy, “Quantum batteries - review chapter,” (2018), arXiv:1805.05507 [quant-ph].

[23] S. Vinjanampathy and J. Anders, Contemporary Physics **57**, 545–579 (2016).

[24] R. Kosloff, Entropy **15**, 2100 (2013).

[25] S. Deffner and S. Campbell, *Quantum Thermodynamics: An introduction to the thermodynamics of quantum information* (Morgan & Claypool Publishers, 2019).

[26] J. Monsel, M. Fellous-Asiani, B. Huard, and A. Auffèves, Physical review letters **124**, 130601 (2020).

[27] F. Kamin, F. Tabesh, S. Salimi, F. Kheirandish, and A. C. Santos, New Journal of Physics **22**, 083007 (2020).

[28] F. Pirmoradian and K. Mølmer, Physical Review A **100**, 043833 (2019).

[29] X. Zhang *et al.*, arXiv preprint arXiv:1812.10139 (2018).

[30] A. Crescente, M. Carrega, M. Sassetti, and D. Ferraro, New Journal of Physics **22**, 063057 (2020).

[31] S. Julià-Farré, T. Salamon, A. Riera, M. N. Bera, and M. Lewenstein, Physical Review Research **2**, 023113 (2020).

[32] B. Mohan and A. K. Pati, Physical Review A **104**, 042209 (2021).

[33] W. Niedenzu, V. Mukherjee, A. Ghosh, A. G. Kofman, and G. Kurizki, Nature communications **9**, 1 (2018).

[34] F. Caravelli, G. Coulter-De Wit, L. P. García-Pintos, and A. Hamma, Physical Review Research **2**, 023095 (2020).

[35] T. P. Le, J. Levinsen, K. Modi, M. M. Parish, and F. A. Pollock, Physical Review A **97**, 022106 (2018).

[36] S. Ghosh, T. Chanda, A. Sen, *et al.*, Physical Review A **101**, 032115 (2020).

[37] F. Zhao, F.-Q. Dou, and Q. Zhao, Phys. Rev. A **103**, 033715 (2021).

[38] D. Rossini, G. M. Andolina, and M. Polini, Physical Review B **100**, 115142 (2019).

[39] S. Zakavati, F. T. Tabesh, and S. Salimi, Physical Review E **104**, 054117 (2021).

[40] S. Ghosh, T. Chanda, S. Mal, A. Sen, *et al.*, Physical Review A **104**, 032207 (2021).

[41] A. C. Santos, A. Saguia, and M. S. Sarandy, Physical Review E **101**, 062114 (2020).

[42] D. Rossini, G. M. Andolina, D. Rosa, M. Carrega, and M. Polini, Physical Review Letters **125**, 236402 (2020).

[43] D. Rosa, D. Rossini, G. M. Andolina, M. Polini, and M. Carrega, Journal of High Energy Physics **2020**, 1 (2020).

[44] Y.-Y. Zhang, T.-R. Yang, L. Fu, and X. Wang, Physical Review E **99**, 052106 (2019).

[45] J. Chen, L. Zhan, L. Shao, X. Zhang, Y. Zhang, and X. Wang, Annalen der Physik **532**, 1900487 (2020).

[46] J. Quach, K. McGhee, L. Ganzer, D. Rouse, B. Lovett, E. Gauger, J. Keeling, G. Cerullo, D. Lidzey, and T. Virgili, arXiv preprint arXiv:2012.06026 (2020).

[47] V. R. Pande, G. Bhole, D. Khurana, and T. Mahesh, Physical Review A **96**, 012330 (2017).

[48] H. G. Krojanski and D. Suter, Physical review letters **97**, 150503 (2006).

[49] A. C. Santos, B. Çakmak, S. Campbell, and N. T. Zinner, Physical Review E **100**, 032107 (2019).

[50] F.-Q. Dou, Y.-J. Wang, and J.-A. Sun, Frontiers of Physics **17**, 1 (2022).

[51] A. C. Santos, Physical Review E **103**, 042118 (2021).

[52] T. S. Mahesh, D. Khurana, V. R. Krithika, G. J. Sreejith, and C. S. S. Kumar, Journal of Physics: Condensed Matter **33**, 383002 (2021).

[53] J.-X. Liu, H.-L. Shi, Y.-H. Shi, X.-H. Wang, and W.-L. Yang, Phys. Rev. B **104**, 245418 (2021).

[54] J. Cavanagh, W. J. Fairbrother, A. G. Palmer III, and N. J. Skelton, *Protein NMR spectroscopy: principles and practice* (Academic press, 1996).